

# Character of Doped Holes in $\text{Nd}_{1-x}\text{Sr}_x\text{NiO}_2$

Tharathep Plienbumrung,<sup>1,2</sup> Michael Schmid,<sup>3</sup> Maria Daghofer,<sup>1,2</sup> and Andrzej M. Oleś<sup>4,5,\*</sup>

<sup>1</sup>*Institute for Functional Matter and Quantum Technologies, University of Stuttgart, Pfaffenwaldring 57, D-70550 Stuttgart, Germany*

<sup>2</sup>*Center for Integrated Quantum Science and Technology, University of Stuttgart, Pfaffenwaldring 57, D-70550 Stuttgart, Germany*

<sup>3</sup>*Waseda Research Institute for Science and Engineering, Waseda University, Okubo, Shinjuku, Tokyo, 169-8555, Japan*

<sup>4</sup>*Max Planck Institute for Solid State Research, Heisenbergstrasse 1, D-70569 Stuttgart, Germany*

<sup>5</sup>*Institute of Theoretical Physics, Jagiellonian University, Profesora Stanisława Łojasiewicza 11, PL-30348 Kraków, Poland*

(Dated: 29 July, 2021)

We investigate charge distribution in the recently discovered high- $T_c$  superconductors, layered nickelates. With increasing value of charge-transfer energy we observe the expected crossover from the cuprate to the local triplet regime upon hole doping. We find that the  $d-p$  Coulomb interaction  $U_{dp}$  plays a role and makes Zhang-Rice singlets less favorable, while the amplitude of local triplets is enhanced. By investigating the effective two-band model with orbitals of  $x^2 - y^2$  and  $s$  symmetries we show that antiferromagnetic interactions dominate for electron doping. The screened interactions for the  $s$  band suggest the importance of rare-earth atoms in superconducting nickelates.

## I. INTRODUCTION: SUPERCONDUCTING INFINITE-LAYERED NICKELATES $\text{NdNiO}_2$

The discovery of Bednorz and Muller [1] started intense search for novel superconductors with high values of the critical temperature  $T_c$ . But in spite of a tremendous effort in the theory, the mechanism responsible for the pairing in cuprates is still unknown [2]. Yet, this is one of the fundamental open problems in modern physics.

Perhaps less spectacular was the recent discovery of superconductivity in infinite-layered  $\text{NdNiO}_2$  doped by Sr [3] as the values of  $T_c$  are "only" close to 15 K [4]. Nevertheless, it gave a new impulse to the theory of high- $T_c$  superconductivity at large. To some extent, the nickelate superconductor family is rather similar to cuprate superconductors [5] as once again two-dimensional (2D) planes of transition metal and oxygen ions play a central role here [6]. With  $\text{Ni}^{1+}$  ions one has again  $d^9$  electronic configuration and similar lattice structure but the apical oxygens are absent. By following the same analysis for a  $\text{NiO}_2$  layer as one performed for a  $\text{CuO}_2$  layer, we expect  $\text{Ni}^{1+}$  to exhibit antiferromagnetic (AFM) order. One finds that the charge-transfer gap in nickelate is larger than that of cuprate [7, 8]. The doped holes reside on oxygen sites in cuprates forming the Zhang-Rice singlet [9]. On the contrary, the doped holes will likely reside on Ni sites in doped  $\text{Nd}_{1-x}\text{Sr}_x\text{NiO}_2$ .

## II. CHARGE-TRANSFER MODEL: $\text{NiO}_2$ MODEL REVISITED

We introduced the multiband  $d-p$  Hamiltonian for a  $\text{NiO}_2$  plane [8] starting from a 2D  $\text{Ni}_4\text{O}_8$   $2 \times 2$  cluster with periodic boundary conditions (PBCs). The basis set includes four orbitals per  $\text{NiO}_2$  unit cell: two  $e_g$  orbitals  $\{3z^2 - r^2, x^2 - y^2\} \equiv \{z, \bar{z}\}$  at each  $\text{Ni}^{1+}$  ion and one bonding  $2p_\sigma$  orbital (either  $2p_x$  or  $2p_y$ ) at each oxygen ion in the

2D plane,

$$\mathcal{H} = H_{dp} + H_{pp} + H_{\text{diag}} + H_{\text{int}}^d + H_{\text{int}}^p. \quad (1)$$

Here the first two terms in the Hamiltonian (1) stand for the kinetic energy:  $H_{dp}$  includes the  $d-p$  hybridization  $\propto t_{pd}$  and  $H_{pp}$  includes the interoxygen  $p-p$  hopping  $\propto t_{pp}$ ,

$$H_{dp} = \sum_{\{m\alpha; j\nu\}, \sigma} \left( t_{pd} \hat{d}_{m\alpha\sigma}^\dagger \hat{p}_{j\nu\sigma} + \text{H.c.} \right), \quad (2)$$

$$H_{pp} = \sum_{\{i\mu; j\nu\}, \sigma} \left( t_{pp} \hat{p}_{i\mu\sigma}^\dagger \hat{p}_{j\nu\sigma} + \text{H.c.} \right), \quad (3)$$

where  $\hat{d}_{m\alpha\sigma}^\dagger$  ( $\hat{p}_{j\nu\sigma}^\dagger$ ) is the creation operator of an electron at nickel site  $m$  (oxygen site  $i$ ) in an orbital  $\alpha \in \{z, \bar{z}\}$  ( $\mu \in \{x, y\}$ ). Here  $z$  and  $\bar{z}$  stand for  $3z^2 - r^2$  and  $x^2 - y^2$  orbitals, while  $\{x, y\}$  stand for  $p_x$  and  $p_y$  orbital. The elements  $\{t_{pd}, t_{pp}\}$  are accompanied by the phase factors which follow from orbital phases [10].

The one-particle (level) energies are included in  $H_{\text{diag}}$ , where we introduce the charge-transfer energy between  $d$  and  $p$  orbitals,

$$\Delta = \varepsilon_d - \varepsilon_p. \quad (4)$$

The model is completed by the Coulomb interactions in the  $d$  and  $p$  orbitals. For the  $d$  electrons,

$$H_{\text{int}}^d = \sum_{m\alpha} U_\alpha n_{m\alpha\uparrow} n_{m\alpha\downarrow} + \left( U' - \frac{1}{2} J_H \right) \sum_i n_{m1} n_{m2} - 2J_H \sum_i \vec{S}_{m1} \cdot \vec{S}_{m2} + J_H \sum_i d_{m1\uparrow}^\dagger d_{m1\downarrow}^\dagger d_{m2\uparrow} d_{m2\downarrow}, \quad (5)$$

where  $\alpha = z, \bar{z}$  stands for  $z^2$  and  $x^2 - y^2$  orbitals.  $d_{m\alpha\sigma}^\dagger$  ( $d_{m\alpha\sigma}$ ) is electron creation (annihilation) operator at site  $m$  in orbital  $\alpha$  with spin  $\sigma$ .  $n_{m\alpha\sigma}$  is a number operator.  $\vec{S}_{m\alpha}$  stands for spin operator in  $\alpha$  orbital at site  $m$ . The two Kanamori parameters to describe the interactions between  $3d$  electrons are  $\{U, J_H\}$ .  $U_\alpha$  is Coulomb repulsion element for  $\alpha$  orbital.  $J_H$  and  $U' = U - 2J_H$  are Hund's exchange and interorbital

\* a.m.oles@fkf.mpi.de

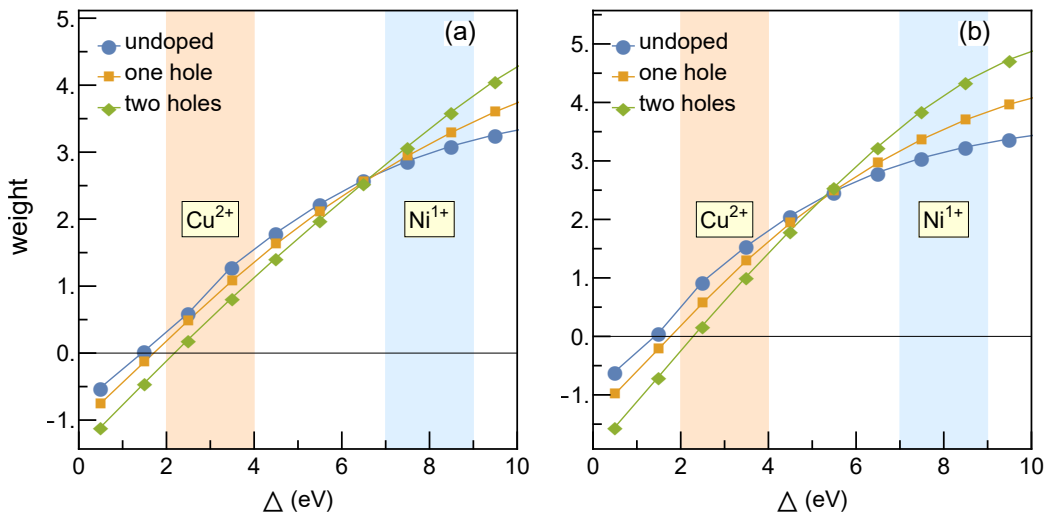


FIG. 1. Doping tendency of NiO<sub>2</sub> model as a function of crystal-field splitting  $\Delta$ : (a)  $U_{dp} = 0$ ; (b)  $U_{dp} = 1$  eV. (Blue) undoped,  $N_{\uparrow} = 2$  and  $N_{\downarrow} = 2$ ; (Orange) one hole doped,  $N_{\uparrow} = 3$ ,  $N_{\downarrow} = 2$ ; (Green) two holes doped,  $N_{\uparrow} = 3$ ,  $N_{\downarrow} = 3$  in Ni<sub>4</sub>O<sub>8</sub> (Cu<sub>4</sub>O<sub>8</sub>) cluster. The nickelate (cuprate) regime is highlighted in blue (orange). The model parameters are given in Table I.

Coulomb interaction [11]. Similar interactions with  $\{U^p, J_H^p\}$  are written for  $p$  electrons.

Figure 1 shows different weight distributions for hole occupations at Ni and O sites for the parameters of Table I. The Ni-O charge-transfer model has been studied via impurity [7] as well as lattice approach [8]. It has been established that the holes in undoped compounds remain within  $d_{x^2-y^2}$  orbitals. Thereby we have assumed that Nd does not contribute to the electronic structure and the system without Sr is a Mott insulator. Doping by Sr gives a doped hole which tends to reside at nickel sites rather than at oxygen sites. The nickelate (cuprate) regime [7] is highlighted in blue (orange) in Fig. 1. In the nickelate regime the holes reside predominantly at Ni sites. This is the essential difference with cuprates where a doped hole (for hole doping) resides predominantly at oxygen and forms a Zhang-Rice singlet [9].

Including intersite Coulomb repulsion  $U_{dp}$  favors the hole occupancy at Ni sites [8] and shifts the doping crossover to lower values of the charge transfer energy  $\Delta$ . All the on-site energies of the Ni( $3d$ ) orbitals have been included in the Ni-O hybridization terms  $t_{pd}$  [7]. Similar results were obtained for finite  $e_g$  orbital splitting, where  $\Delta_z = 1$  eV should be considered the upper limit.

The NiO<sub>2</sub> compound is a Mott-Hubbard insulator. It is then possible to replace the charge-transfer model by the  $d$ -only Hubbard model. The effective Ni-Ni hoppings can be derived from second-order perturbation theory [12]. The next question is on which  $d$ -orbitals the doped holes are?

TABLE I. Parameters of the NiO<sub>2</sub> charge-transfer model (all in eV) used in [8].

$t_{pd}$	$t_{pp}$	$\Delta$	$U_z = U_{\bar{z}}$	$J_H$	$U_p$	$J_H^p$
1.30	0.55	7.0	8.4	1.2	4.4	0.8

The asymmetric distribution of holes suggests that one could replace the Ni-O model (1) with Ni  $d$ -only model as oxygen  $p$ -orbitals become unimportant. The DFT calculation shows the band structure of NdNiO<sub>2</sub> that two bands are crossing Fermi level. In the orbital-resolved band structure, the lower band has  $d_{x^2-y^2}$  character and the upper band contains both Nd and Ni contributions. The large charge transfer energy as well as the presence of electron pocket at  $\Gamma$  are the two striking features of the nickelate compound. The empty  $5d$  states of Nd are responsible for providing electron pocket. The empty  $5d$  states are below the Fermi level, in other words, these states provide the hole states into Ni band by the so-called 'self-doped' effect [13]. Furthermore, the  $5d$  states was shown to be hybridized with Ni apical orbitals i.e.,  $3d_{z^2}$  and  $4s$  orbitals [14] lead us to construct the effective two-band model consisting of Ni in-plane orbital,  $d_{x^2-y^2}$ , and Ni off-plane orbital, the modified  $s$  orbital. In this work, we present the character of doped holes in the realistic two-band model of NdNiO<sub>2</sub> compound.

### III. ELECTRONIC STRUCTURE CALCULATIONS

The *ab initio* electronic structure calculations using density functional theory (DFT) were performed with the Quantum Espresso code [15–17] using a plane-wave pseudopotential method, combining a projector augmented wave method [18] and a specific choice of pseudopotentials [19]. Within this work we chose an energy cutoff of 600 eV and a  $\Gamma$ -centered Brillouin zone mesh of  $16 \times 16 \times 16$ . For all calculations we used the same crystal structure published in Ref. [20]. The two-band model is derived by performing a Wannier projection onto the DFT band structure as implemented within the Wannier90 interface [21], including onsite energies and hopping parameters of each Wannier orbital. The projection was

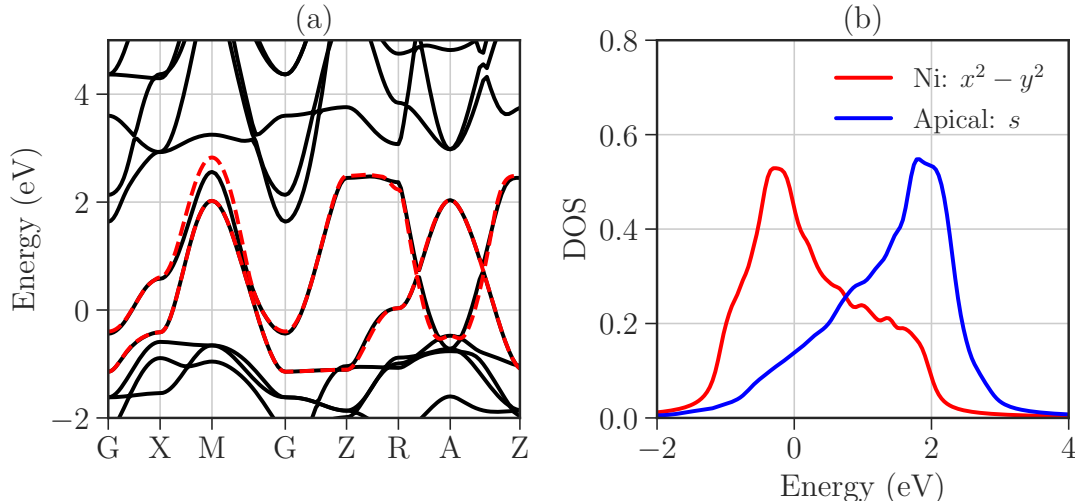


FIG. 2. DFT band structure and DOS of the Wannier Hamiltonian: (a) DFT band structure (black solid lines) compared with Wannier band structure (red dashed lines), and (b) Wannier DOS for the Ni( $x^2 - y^2$ ) (red) and apical Ni( $s$ ) orbital (blue).

performed onto a Ni( $x^2 - y^2$ ) and an apical Ni( $s$ ) Wannier orbital within an energy window ranging from  $-2.0$  to  $4.0$  eV. The DFT band structure, represented here by the projected Wannier bands, and its density of states (DOS), are shown in Fig. 2. Panel Fig. 2a shows the DFT band structure (black lines) and Wannier bands (red dashed lines). The right panel Fig. 2b contains the resulting Wannier DOS around the Fermi energy for the bands of two symmetries:  $x^2 - y^2$  and  $s$ . Our result qualitatively matches previous studies [14, 20].

The Wannier Hamiltonian is given within the real space notation and is of the form,

$$\mathcal{H}(\mathbf{R}) = \sum_{ij\alpha\sigma} t_{ij\alpha}(\mathbf{R}) c_{i\alpha\sigma}^\dagger c_{j\alpha\sigma}. \quad (6)$$

TABLE II. Hoppings parameters for the two-band model (all in eV) used in ED calculations.

$(x, y, z)$	$t_{ijk}^{\alpha\beta}$
(0,0,0)	$\begin{pmatrix} 0.2 & 0 \\ 0 & 1.2 \end{pmatrix}$
(1,0,0)	$\begin{pmatrix} -0.380 & -0.050 \\ -0.050 & -0.031 \end{pmatrix}$
(0,1,0)	$\begin{pmatrix} -0.380 & 0.050 \\ 0.050 & -0.031 \end{pmatrix}$
(0,0,1)	$\begin{pmatrix} -0.039 & 0 \\ 0 & -0.076 \end{pmatrix}$
(1,1,0)	$\begin{pmatrix} 0.088 & 0 \\ 0 & -0.111 \end{pmatrix}$
(1,0,1)	$\begin{pmatrix} 0.001 & -0.009 \\ -0.009 & -0.252 \end{pmatrix}$
(0,1,1)	$\begin{pmatrix} 0.001 & 0.009 \\ 0.009 & -0.252 \end{pmatrix}$
(1,1,1)	$\begin{pmatrix} 0.015 & 0 \\ 0 & 0.056 \end{pmatrix}$

The basis is ordered following the convention  $\{d_{x^2-y^2}, s\}$ . Explicit numerical values for the hopping parameters are given in Table II for the terms with leading contributions, i.e., terms larger than 0.001 (the other terms were neglected). Note that the relation  $\mathcal{H}(-\mathbf{R}) = \mathcal{H}^T(\mathbf{R})$  holds for Wannier models. As a consequence, both terms (for distances  $\mathbf{R}$  and  $-\mathbf{R}$ ) need to be included in further calculations. From  $\mathcal{H}(\mathbf{R})$  a tight-binding Hamiltonian can be constructed by applying a Fourier transformation of the form,

$$\mathcal{H}_{ij}(\mathbf{k}) = \sum_{\mathbf{R}} e^{i\mathbf{k}\cdot\mathbf{R}} \mathcal{H}_{ij}(\mathbf{R}), \quad (7)$$

where  $\mathbf{R}$  describes the distances of the Wannier orbitals  $|i-j|$  and is typically represented in terms of the lattice vectors.

#### IV. EFFECTIVE TWO-BAND HAMILTONIAN

Following the idea of neglecting oxygen orbitals, we construct an effective model containing only Ni( $3d$ ) orbitals. The band structure calculation shows that only two bands contribute at Fermi level. Therefore, the two-band model of nickelates is capable of reproducing the physics of nickelates. It consists of  $x^2 - y^2$  orbital and the  $s$  orbital which includes rare-earth  $5d$  states and Ni apical orbitals.

We consider the two-band Hamiltonian  $H = H_{\text{kin}} + H_{\text{int}}$ . The kinetic part is

$$H_{\text{kin}} = \sum_{i\alpha\sigma} \epsilon_\alpha a_{i\alpha\sigma}^\dagger a_{i\alpha\sigma} + \sum_{ij\alpha\beta\sigma} t_{ij}^{\alpha\beta} a_{i\alpha\sigma}^\dagger a_{j\beta\sigma}, \quad (8)$$

while the interactions are given in a similar way to Eq. (5). The orbitals  $x^2 - y^2$  and  $s$  have the diagonal energies  $\epsilon_\alpha$ , being 0 and  $\epsilon$ . The bands are constructed following Ref. [14]. The oxygen  $2p$  orbitals are included implicitly in  $x^2 - y^2$

ones. Note that one should not confuse here  $x^2 - y^2$  symmetry with  $\text{Ni}(x^2 - y^2)$  orbital. The former is an effective orbital including in-plane oxygen while the latter is solely a  $\text{Ni}(3d)$  orbital. The  $s$  orbital contains contributions from  $\text{Nd}(5d)$ ,  $\text{Ni}(3d_{z^2})$  and  $\text{Ni}(4s)$  orbitals. The symmetry of this hybrid orbital is the same as that of atomic  $s$  orbital.

Instead of  $\text{Nd}(4f)$  electronic states, the empty  $\text{Nd}(5d)$  orbitals are responsible for the striking electron pocket at the  $\Gamma$  point in the band structure [5]. The Nd atoms are originally located in the off-plane direction of Ni-O plane. In this effective model the rare-earth atoms are included into Ni atoms via  $s$  orbital, indicating the model is three-dimensional and the Coulomb interaction as well as Hund's coupling need to be screened. For instance, the two electrons sitting within  $s$  orbital could be located either at Nd or at Ni atom. Therefore, the Coulomb repulsion between these two electrons within the  $s$  orbital is reduced. We introduce a parameter  $\alpha \in [0, 1]$  to represent the reduced Coulomb interaction and Hund's coupling, i.e.,  $U_2 = \alpha U_1$  and  $J = \alpha J_H$ .  $\alpha = 1(0)$  stands for weak (strong) screening effect from rare-earth atoms, and we consider two parameter sets *A* and *B*, given in Table III. We study the effective two-band model via Lanczos algorithm [22] on a  $2 \times 2 \times 2$  unit cell.

The undoped nickelate corresponds to quarter-filling, i.e., 8 electrons. The stoichiometric compound has  $d^9$  configuration, where  $\text{Ni}(x^2 - y^2)$  orbital is half-filled, and the weak hybridization of Ni and Nd causes  $\text{Ni}(x^2 - y^2)$  orbital to be away from half-filling and creates the self-doping effect [13, 23]. The Ni-Ni hopping integrals are obtained via fitting Wannier functions on DFT band calculation. We aim to address the question: where the doped holes are located in the two-band model?

In the absence of electron hoppings Hamiltonian, the ground state is a trivial antiferromagnet where  $x^2 - y^2$  orbital is half-filled and the two canonical AFM phases, *C*-AFM and *G*-AFM, are degenerate. Including hopping elements to further neighbors leads to metallic behavior. In one-band Hubbard model the metal-insulator transition occurs when  $U = 2zt$ , where  $z = 4$  is the number of neighbors in the 2D plane. Similarly, the two-band description can lead to partial orbital-selective Mott transition where one band is insulating and the other one remains metallic. In the one-band version, the two relevant configurations are singly occupied or form double occupation within a single site. The quarter filling two-band version, however, contains several possible configurations where the lowest energy is still a single occupancy followed by a local triplet state with energy  $(U - 3J_H)$  [11].

TABLE III. Parameters of the two-band model (all in eV) used in exact diagonalization calculations. The reference energies for the two bands of  $x^2 - y^2$  and  $s$  symmetry are 0 and  $\epsilon$ , respectively.

set	$\epsilon$	$t$	$U_1$	$J_H$
<i>A</i>	1.21	0.38	8.0	1.2
<i>B</i>	1.21	0.38	4.0	0.6

## V. RESULTS AND DISCUSSION

We begin with electronic density distribution on  $2 \times 2 \times 2$  clusters obtained by exact diagonalization with twisted boundary condition (TBC). The hopping parameters used here are given in Table II. With PBC, one requires hopping integrals  $t_{ij}^{\alpha\beta}$  to be scaled by the factor of 1/2 due to double-counting at the boundary. To avoid this additional factor in the hopping terms, we replace the PBC with TBC. Instead of having a constant phase  $t_{N+i} = t_i$  as in PBCs, the hopping terms at the boundary are modified by twisted angles  $(\phi_x, \phi_y, \phi_z)$ , giving  $t_{N+i} = e^{i\vec{\phi} \cdot \vec{r}_i} t_i$ ; for more details see Refs. [24, 25]. The PBC corresponds to  $(0, 0, 0)$ , while  $(\pi, \pi, \pi)$  is obtained for the anti-periodic boundary condition. In what follows, the observables are obtained by averaging over several twisted angles.

In Figs. 3a-3b, we show the undoped orbital-resolved densities, i.e., the electron occupancy within each orbital:  $x^2 - y^2$  (predominantly occupied) and  $s$  (it usually has decent amount of electrons). Finite occupancy of  $s$  orbital is expected due to self-doping effect. We further see that increasing of the parameter  $\alpha$  causes the occupation on  $x^2 - y^2$  orbital to approach half-filling. Once the  $x^2 - y^2$  orbitals are almost half-filled, we show below that the *G*-AFM ground state is the only dominant magnetic ground state. Including screening effect into  $x^2 - y^2$  orbital by lowering its Coulomb interaction gives this orbital as slightly more favorable, see also Fig. 3a-3b.

By adding one hole, we see that both orbitals can be occupied by holes depending on how strong the screening effects of  $s$  orbital are, see Figs. 3c-3d. The screening effect on  $x^2 - y^2$  orbitals makes little changes in the one-hole case. An interesting scenario arises when two holes are added into the undoped Ni-O plane. When taking the screening effect into account, holes are effectively occupying the  $x^2 - y^2$  orbital regardless of the parameter  $\alpha$ .

Theoretical studies based on  $\text{Ni}(e_g)$  bands [8, 13, 23] have suggested that high-spin  $S = 1$  state  $\text{Ni}^{2+}$  is favorable for hole doping. In contrast, RIXS measurements [26] show that two holes are residing mainly within  $\text{Ni}(x^2 - y^2)$ . Due to the limitation of the measurement, we cannot determine the occupation of the rare-earth  $5d$  states. The difference between the predictions of the theoretical model and the experiment arises from the rare-earth atoms. In the  $\text{Ni}(e_g)$  with  $d^8$  configuration, the  $x^2 - y^2$  is half-filled and forming a high-spin state together with another  $3d$  orbital with energy  $(U - 3J_H)$  [8]. This energy is significantly smaller than the energy  $U$  for a low-spin  $d^8$  state. On the contrary, the  $s$  orbital, in the hole picture, has lower energy than  $x^2 - y^2$  orbital and the quarter-filling of electrons corresponds to  $\frac{3}{4}$ -filling by holes via particle-hole transformation. In this case, the  $s$  orbital is filled by holes and leaves half-filled  $x^2 - y^2$  orbital—then holes reside mainly on  $x^2 - y^2$  orbital. This intuitive picture of hole configuration requires the  $x^2 - y^2$  to be nearly half-filled, in other words, it suggests that the ground state is a strong antiferromagnet as in cuprates [9, 27]. However, NMR experiments [28, 29] report no observation of long-range AFM order in the  $R\text{NiO}_2$  ( $R=\text{Nd,La}$ ) down to 2 K.

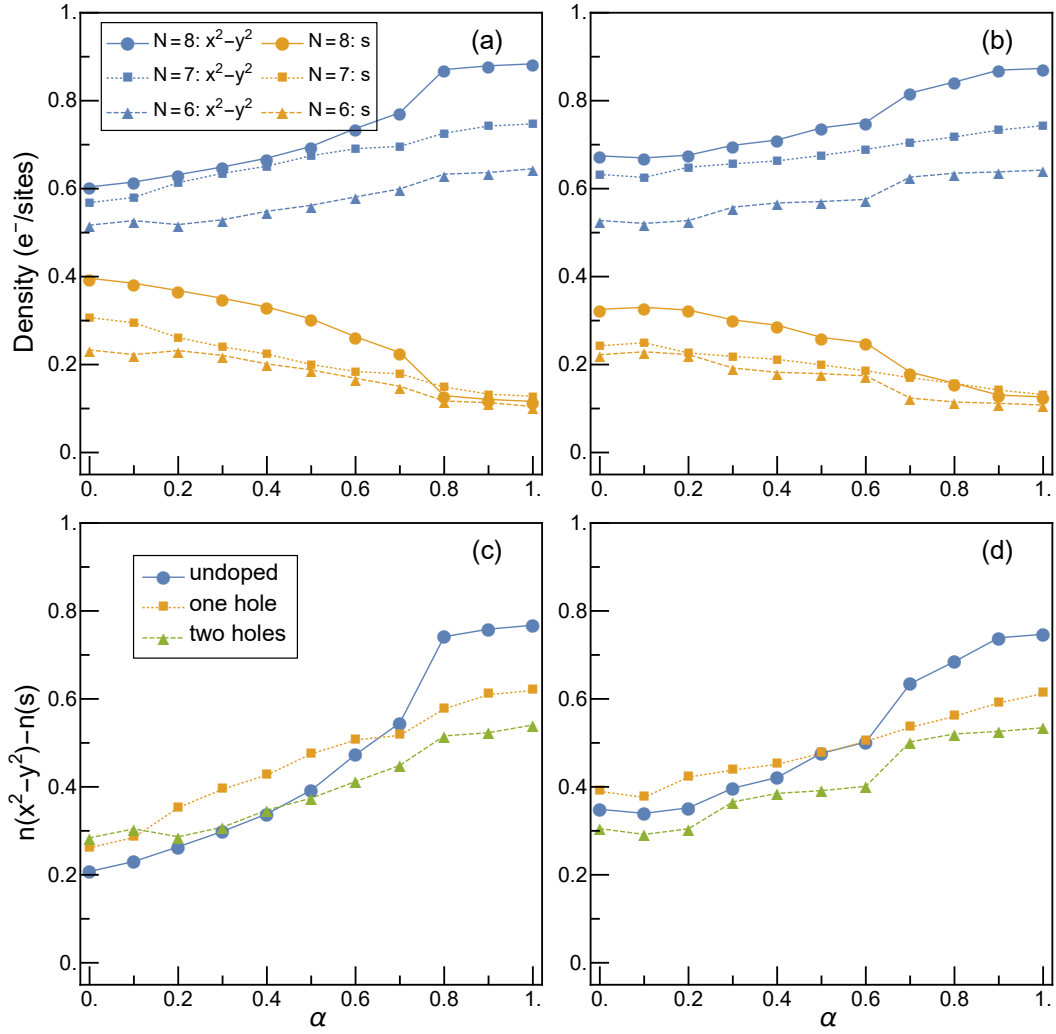


FIG. 3. Orbital-resolved electron densities as obtained for: (a) set A, and (b) set B, see Table III. Strongly anisotropic electron distribution over the  $d_{x^2-y^2}$  and  $s$  orbitals is favored when the interactions are screened by  $\alpha > 0.5$ , as shown for: (c) set A, and (d) set B.

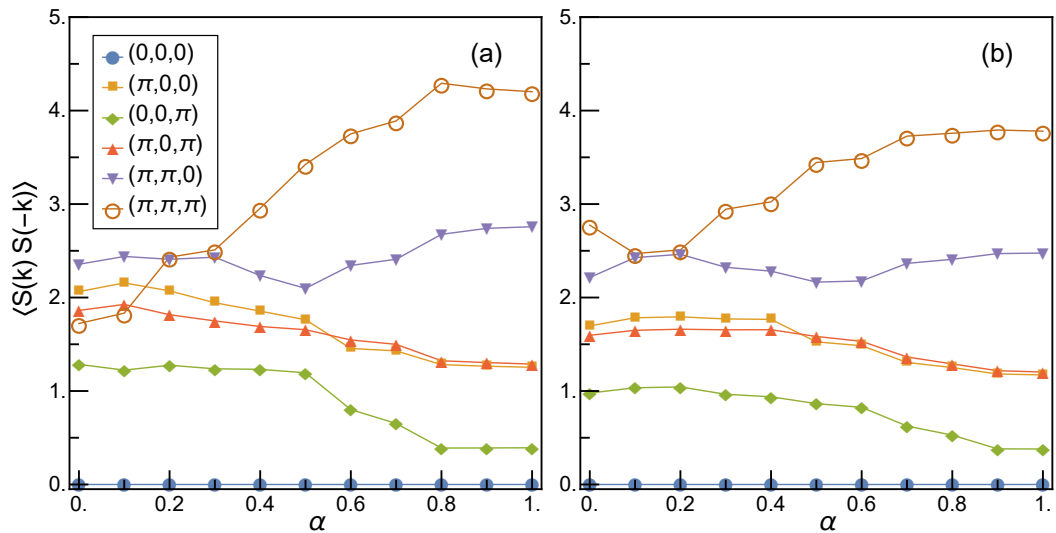


FIG. 4. Spin structure factor (9) of the three-dimensional two-band model, as obtained for: (a) set A, and (b) set B, see Table III.

According to DFT+*si*cDMFT approach [23], the paramagnetic ground state has the lowest energy followed by *C*-AFM



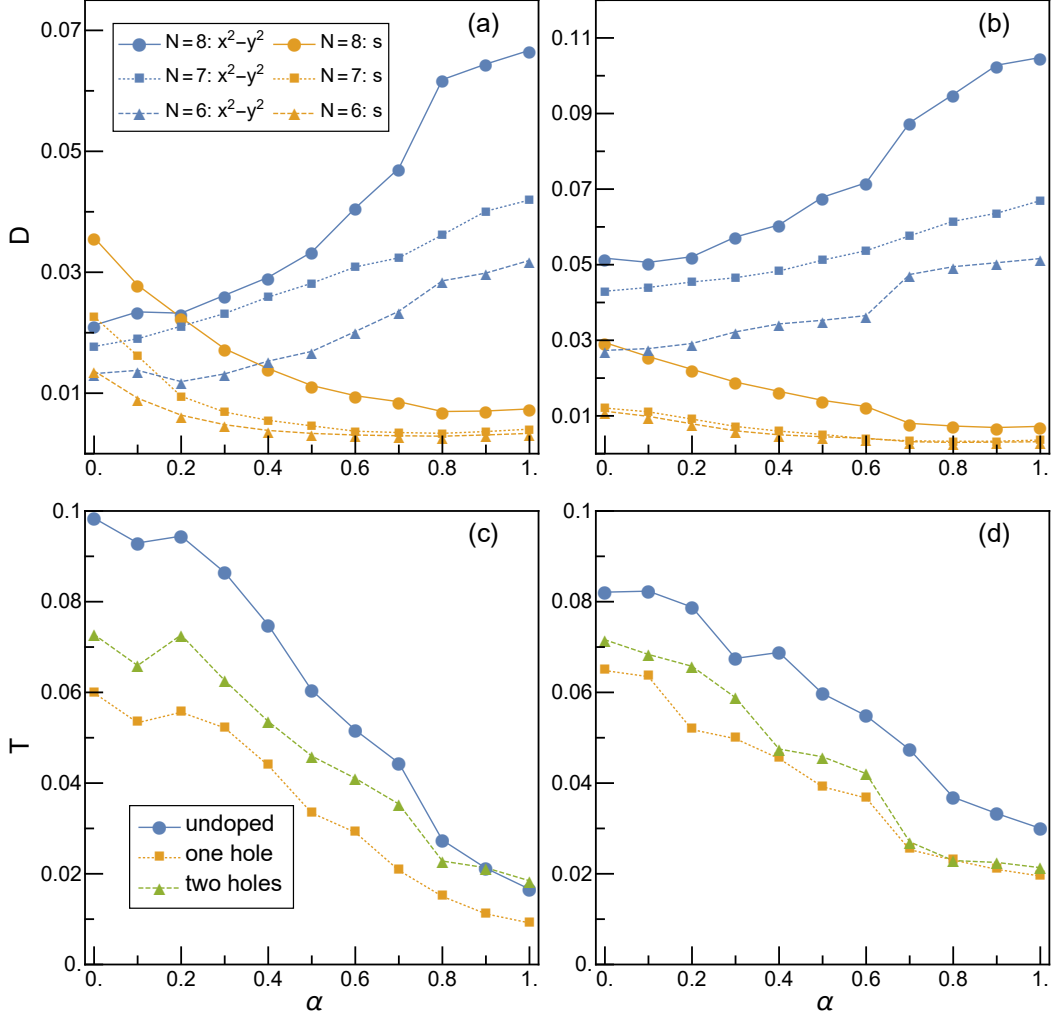


FIG. 5. Competition between low-spin and high-spin states as obtained for the parameters of: (a,c) set A, and (b,d) set B, see Table III. Panels (a) and (b) show local double occupancy  $D_\alpha$  in each  $\alpha = x^2 - y^2, s$  orbital, while panels (c) and (d) show local triplet states  $T$ .

with energy difference about 20 meV/atom and  $G$ -AFM with energy 105 meV/atom. The  $C$ -AF state has parallel spins along the  $c$  axis, while  $G$ -AFM phase has antiparallel spin alignment to its nearest neighbor in all directions. To address the magnetic order in this two-band model, the spin structure factor of undoped profile,

$$\langle S(k)S(-k) \rangle = \sum_{ij} e^{i\vec{k}(\vec{r}_i - \vec{r}_j)} \langle \vec{S}_i \cdot \vec{S}_j \rangle, \quad (9)$$

is shown in Fig. 4. With this small cluster size we can observe only six relevant  $\mathbf{k}$ -points in the Brillouin zone. The spin structure factor at  $(\pi, \pi, \pi)$  is enhanced as the  $x^2 - y^2$  is close to half-filled band, indicating that  $G$ -AFM order is favored, see Fig. 4. At small  $\alpha$ , the spin structure factor (9) shows a competition between several magnetic ordered states, dominated by  $(\pi, \pi, 0)$  and  $(\pi, \pi, \pi)$ . In the recent  $x$ -ray scattering experiment [30], the existence of AFM correlations was confirmed but the small cluster size prevents us from concluding whether AFM long-range order could be stable in this regime.

The screening effect from rare-earth atoms [13, 31] could be responsible for the competition of magnetic orders. At small  $\alpha$  where the screening effect from rare-earth is strong, the electrons tend to form on-site triplets with energy  $\epsilon + \alpha(U_1 - 3J_H)$  [8], coexisting with singly occupied  $x^2 - y^2$  orbitals. Then increasing  $\alpha$  enhances the interactions on  $s$  orbitals and the on-site triplet energy surpasses the bandwidth of  $s$  orbital, i.e.,  $\epsilon + \alpha(U_1 - 3J_H) > 2zt$  ( $z = 4$ ). The largest hopping elements are the in-plane hoppings along  $x$  and  $y$  direction of  $x^2 - y^2$  orbital. Another transition then occurs when the on-site triplet energy overcome the bandwidth of  $x^2 - y^2$  orbital, becoming a Mott insulator.

Figure 5 shows the competition between low-spin and high-spin states in  $\text{NiO}_2$  planes of the novel Ni-layered superconductors for decreasing number of holes, i.e., for electron doping. Here we use  $D_\alpha = \frac{1}{N} \sum_i \langle n_{i\alpha\uparrow} n_{i\alpha\downarrow} \rangle$  and  $T = \frac{1}{N} \sum_i \langle \frac{3}{4} + \vec{S}_{i1} \cdot \vec{S}_{i2} \rangle$ , where  $N$  is the number of lattice sites. We show here that the double occupancy  $D_\alpha$  is reduced with decreasing number of holes in the plane. Similarly, the

amplitude of high-spin states  $T$  at Ni sites is reduced in this regime. So we conclude that electron doped materials have low-spin configuration. On the contrary, hole doping may favor locally high-spin ( $S = 1$ ) states instead of singlet ( $S = 0$ ) double occupancies of  $x^2 - y^2$  orbitals [8].

## VI. SUMMARY AND CONCLUSIONS

In summary, we have replaced the half-filled  $d - p$  charge-transfer model by the effective two-band model at quarter-filling. The characters of each band are given by  $x^2 - y^2$  and  $s$  symmetry. The contributions of Nd and Ni atoms to  $s$  orbital lead to the reduction of Hund's exchange and Coulomb repulsion. Its strength is scaled by the parameter  $\alpha$ . The model shows the three competing phases: metal, orbital-selective and Mott insulator. The Mott insulator is realized when the splitting between on-site triplet and singly occupied state is larger than the size of the bandwidth, similar to one-band Hubbard model. It is followed by the orbital-selective Mott insulator where the orbital splitting separates the  $s$  and  $x^2 - y^2$  bandwidth.

The nonmagnetic ordering is unlikely within this small unit cell and only AFM configuration can be realized. While the  $G$ -AFM phase is clearly dominating at large  $\alpha$ , the competition between  $C$ -AFM and  $G$ -AFM is found at low  $\alpha$  where the on-site triplet competes with AFM ground state, indicating the tendency toward AFM ordering. The holes are doped differently among the three phases. In metallic phase, the itinerant  $s$  orbital is favorable for holes. On the other hand, in the

orbital-selective phase, the situation is slightly complicated while adding one hole favors  $s$  orbital but adding two holes can effectively lead again to  $x^2 - y^2$  occupation, as in the Mott insulating phase.

When the screening effect on  $x^2 - y^2$  orbital is included, the stability of orbital-selective phase is enhanced and metallic phase vanishes. The two-band model at quarter-filling, therefore, connects the two controversial scenerios of which orbitals preferred by doped-holes via the parameter  $\alpha$ . The parameter somehow represents the screening effect from rare-earth orbital, showing the importance of rare-earth atoms for the electronic structure of superconducting nickelate.

**Authors' Contributions:** Tharathep Plienbumrung performed numerical analysis of the two-band model. The two-band model was derived from the  $d - p$  charge-transfer model by Michael Schmid. All authors selected the relevant information, analyzed the predictions of the theory versus experimental data, developed the interpretation of the numerical results, and wrote the manuscript.

**Funding:** T. P. acknowledges Development and Promotion of Science and Technology Talents Project (DPST). A. M. Oleś kindly acknowledges Narodowe Centrum Nauki (NCN, National Science Centre, Poland) Project No. 2016/23/B/ST3/00839.

**Acknowledgments:** We would like to thank Andres Greco, Peter Horsch, Krzysztof Rościszewski, and George A. Sawatzky for many insightful discussions. A. M. Oleś is grateful for the Alexander von Humboldt Foundation Fellowship (Humboldt-Forschungspreis).

**Conflicts of Interest:** We declare no conflicts of interest.

- 
- [1] Bednorz, J.G.; Muller, K.A. Possible high- $T_c$  superconductivity in the Ba-La-Cu-O system. *Z. Phys. B* **1986**, *64*, 189-193.
- [2] Keimer, B.; Kivelson, S.A.; Norman, M.R.; Uchida, S.; Zaanen, J. From quantum matter to high-temperature superconductivity in copper oxides. *Nature* **2011**, *518*, 179-186.
- [3] Li, D.; Lee, K.; Wang, B.Y.; Osada, M.; Crossley, S.; Lee, H.R.; Cui, Yi; Hikita, Y.; Hwang, H.Y. Superconductivity in an infinite-layer nickelate. *Nature* **2019**, *572*, 624-627.
- [4] Li, D.; Wang, B.Y.; Lee, K.; Harvey, S.P.; Osada, M.; Goodge, B.H.; Kourkoutis, L.F.; Hwang, H.Y. Superconducting Dome in  $\text{Nd}_{1-x}\text{Sr}_x\text{NiO}_2$  Infinite Layer Films. *Phys. Rev. Lett.* **2020**, *125*, 027001.
- [5] Botana, A.S.; Norman, M.R. Similarities and differences between  $\text{LaNiO}_2$  and  $\text{CaCuO}_2$  and implications for superconductivity. *Phys. Rev. X* **2020**, *10*, 011024.
- [6] Jarlborg, T.; Bianconi, A. Multiple Electronic Components and Lifshitz Transitions by Oxygen Wires Formation in Layered Cuprates and Nickelates. *Condensed Matter* **2019**, *4*, 15.
- [7] Jiang, M.; Berciu, M.; Sawatzky, G.A. Critical Nature of the Ni Spin State in Doped  $\text{NdNiO}_2$ . *Phys. Rev. Lett.* **2020**, *124*, 207004.
- [8] Plienbumrung, T.; Daghofer, M.; Oleś, A.M. Interplay between Zhang-Rice singlet and high-spin states in a model for doped  $\text{NiO}_2$  planes. *Phys. Rev. B* **2021**, *103*, 104513.
- [9] Zhang, F.C.; Rice, T.M. Effective Hamiltonian for the superconducting Cu Oxides. *Phys. Rev. B* **1988**, *37*, 3759-3761.
- [10] Arrigoni, E.; Aichhorn, M.; Daghofer, M.; Hanke, W. Phase diagram and single-particle spectrum of  $\text{CuO}_2$  high- $T_c$  layers: Variational cluster approach to the three-band Hubbard model. *New J. Phys.* **2009**, *11*, 055066.
- [11] Oleś, A.M. Antiferromagnetism and correlation of electrons in transition metals. *Phys. Rev. B* **1983**, *28*, 327-339.
- [12] Hu, L.-H.; Wu, C. Two-band model for magnetism and superconductivity in nickelates. *Phys. Rev. Research* **2019**, *1*, 032046.
- [13] Zhang, G.-M.; Yang, Y.F.; Zhang, F.C. Self-doped Mott insulator for parent compounds of nickelate superconductors. *Phys. Rev. B* **2020**, *101*, 020501(R).
- [14] Adhikary, P.; Bandyopadhyay, S.; Das, T.; Dasgupta, I.; Saha-Dasgupta, T. Orbital selective superconductivity in a two-band model of infinite-layer nickelates. *Phys. Rev. B* **2020**, *102*, 100501(R).
- [15] Giannozzi, O.; Baroni, S.; Bonini, N.; Calandra, M.; Car, R.; Cavazzoni, C.; Ceresoli, D.; Chiarotti, G.L.; Cococcioni, M.; Daboet, I.; et al. QUANTUM ESPRESSO: A modular and open-source software project for quantum simulations of materials. *J. Phys.: Condensed Matter* **2009**, *21*, 395502.
- [16] Giannozzi, O.; Andreussi, O.; Brumme, T.; Bunau, O.; Buongiorno Nardelli, M.; Calandra, M.; Car, R.; Cavazzoni, C.; Ceresoli, D.; Cococcioni, M.; et al. Advanced capabilities for materials modelling with Quantum ESPRESSO. *J. Phys.: Condensed Matter* **2017**, *29*, 465901.

- [17] Giannozzi, O.; Barone, P.; Bonfà, P.; Brunato, D.; Car, R.; Carnimeo, I.; Cavazzoni, C.; de Cironcoli, S.; Delugas, P.; Ruffino, F.F.; et al. Quantum ESPRESSO toward the exascale. *J. Chem. Phys.* **2020**, *152*, 154105.
- [18] Lejaeghere, K.; Bihlmayer, G.; Björkman, T.; Blaha, P.; Blügel, S.; Blum, V.; Caliste, D.; Castelli, I.E.; Clark, S.J.; Dal Corso, A.; et al. Reproducibility in density functional theory calculations of solids. *Science* **2016**, *351*, aad3000.
- [19] Dal Corso, A. Pseudopotentials periodic table: From H to Pu. *Comp. Mat. Science* **2014**, *95*, 337-350.
- [20] Gu, Y.; Zhu, S.; Wang, X.; Hu, J.; Chen, H. A substantial hybridization between correlated Ni-*d* orbital and itinerant electrons in infinite-layer nickelates. *Communications Phys.* **2020**, *3*, 84.
- [21] Pizzi, G.; Zhu, S.; Wang, X.; Hu, J.; Chen, H. Wannier90 as a community code: new features and applications. *J. Phys.: Condensed Matter* **2020**, *32*, 165902.
- [22] Koch, E. The Lanczos Method, in: The LDA+DMFT approach to strongly correlated materials. edited by E. Pavarini, E. Koch, D. Vollhardt, and A. Lichtenstein. Forschungszentrum Jülich, **2011**.
- [23] Lechermann, F. Doping-dependent character and possible magnetic ordering of NdNiO<sub>2</sub>. *Phys. Rev. Materials* **2021**, *5*, 044803.
- [24] Shiroshi, M.; Wadati, M. Integrable boundary conditions for the one-dimensional Hubbard model. *J. Phys. Soc. Jpn.* **2012**, *66*, 2288-2301.
- [25] Poilblanc, D. Twisted boundary conditions in cluster calculations of the optical conductivity in the two-dimensional lattice models. *Phys. Rev. B* **1991**, *44*, 9562-9581.
- [26] Rossi, M.; Lu, H.; Nag, A.; Li, D.; Osada, M.; Lee, K.; Wang, B.Y.; Agrestini, S.; Garcia-Fernandez, M.; Chuang, Y.-D.; et al. Orbital and Spin Character of Doped Carriers in Infinite-Layer Nickelates. ArXiv:2011.00595 **2020**.
- [27] Anisimov, V. I.; Bukhvalov, D.; Rice, T. M. Electronic structure of possible nickelate analogs to the cuprates. *Phys. Rev. B* **1999**, *59*, 7901-7906.
- [28] Hayward, M. A.; Green, M. A.; Rosseinsky, M. J.; Sloan, J. Sodium Hydride as a Powerful Reducing Agent for Topotactic Oxide Deintercalation: Synthesis and Characterization of the Nickel(I) Oxide LaNiO<sub>2</sub>. *J. Am. Chem. Soc.* **1999**, *121*, 8843-8854.
- [29] Hayward, M. A.; Rosseinsky, M. J. Synthesis of the infinite layer Ni(I) phase NdNiO<sub>2+x</sub> by low temperature reduction of NdNiO<sub>3</sub> with Sodium Hydride. *Solid State Sciences* **2003**, *5*, 839-850.
- [30] Lu, H.; Rossi, M.; Nag, A.; Osada, M.; Li, D.F.; Lee, K.; Wang, B.Y.; Garcia-Fernandez, M.; Agrestini, S.; Shen, Z.X.; et al. Magnetic excitations in infinite-layer nickelates. *Science* **2021**, *373*, 213-216.
- [31] Sakakibara, H.; Usui, H.; Suzuki, K.; Kotani, T.; Aoki, H.; Kuroki, K. Model Construction and a Possibility of Cupratelike Pairing in a New *d<sup>9</sup>* Nickelate Superconductor (Nd,Sr)NiO<sub>2</sub>. *Phys. Rev. Lett.* **2020**, *125*, 077003.